Article

B$_4$C-Al Composites Fabricated by the Powder Metallurgy Process

Ling Zhang, Jianmin Shi, Chunlei Shen, Xiaosong Zhou * , Shuming Peng and Xinggui Long

Institute of Nuclear Physics and Chemistry, China Academy of Engineering Physics, Mianyang 621900, China; zlxs77@126.com (L.Z.); shijianmin1986@163.com (J.S.); scl19860217@126.com (C.S.); pengshuming@caep.cn (S.P.); xingguil@caep.cn (X.L.)

* Correspondence: zlxs77@163.com; Tel.: +86-816-2497405

Featured Application: Neutron absorber materials are used in spent-fuel storage racks, storage, and transportation casks to control the reactivity of spent nuclear fuel, allowing the storage and shipment of spent fuel at maximum packing density. Due to the large thermal neutron absorption cross-section of the nuclide B-10 and the excellent mechanical performance of aluminum, B$_4$C-Al composites have the potential to serve as the neutron absorber as well as the structural function in fuel racks. This work provides an efficient method to fabricate the homogeneously mixed B$_4$C-Al composites with superior yield and tensile strength.

Abstract: Due to the large thermal neutron absorption cross section of ^{10}B, B$_4$C-Al composites have been used as neutron absorbing materials in nuclear industries, which can offer not only good neutron shielding performance but also excellent mechanical properties. The distribution of B$_4$C particles affects the mechanical performance and efficiency of the thermal neutron absorption of the composite materials. In this study, 15 wt % B$_4$C-Al and 20 wt % B$_4$C-Al composites were prepared using a powder metallurgy process, i.e., ball milling followed by pressing, sintering, hot-extrusion, and hot-rolling. The yield and tensile strengths of the composites were markedly increased with an increase in the milling energy and the percentages of B$_4$C particles. Microstructure analysis and neutron radiography revealed that the high-energy ball milling induced the homogeneous distribution of B$_4$C particles in the Al matrix and good bonding between the Al matrix and the B$_4$C particles. The load transfer ability and mechanical properties of the composites were consequently improved. The results showed the high-energy ball milling process is an appropriate fabrication procedure to prevent the agglomeration of the reinforcement particles even if the matrix to reinforcement particle size ratio was nearly 10.

Keywords: B$_4$C-Al composites; high-energy ball milling; mechanical property; neutron radiography

1. Introduction

Aluminum-based metal matrix composites (MMCs) generally show low density, low coefficient of thermal expansion, and high specific strength and modulus, etc.; therefore, they have been widely used in aerospace, military weapons, structural applications, and automobile products [1–7]. Boron carbide (B$_4$C) has a low density (2.52 g/cm^3), extremely high hardness, excellent chemical resistance, and a high neutron absorption cross-section [1,2,8–13]. B$_4$C-Al composites have the potential to combine the high toughness and hardness of B$_4$C with the good ductility and lightweight structure of the Al matrix; thus, they have been recently investigated for various applications in high-strength structural materials, armor plate materials, substrate materials for computer hard disks, and neutron absorber materials in nuclear industries [7,11,14,15].

Generally, the distribution of the reinforcing particles significantly affects the performance of particulate reinforced MMCs [3,8]. B_4C, Al_2O_3, and SiC-reinforced Al matrix composites were previously fabricated using a liquid melt-stirring process in air [5]. Below 1100 °C the wetting between Al and B_4C is bad, so it is hard to prepare Al-B_4C composites by dispersing particles into the liquid phase. In order to improve the wettability of reinforcing particles and enhance their incorporation into molten aluminium, reinforcing particles are often coated or heat treated in advance [2]. The B_4C reacts drastically with molten Al, producing various binary and ternary compounds, such as Al_3BC, AlB_2, Al_4C_3, etc., which are detrimental to the mechanical properties of the composites.

On the other hand, the clustering of the reinforced particles tends to takes place when the particle size of the matrix exceeds that of the reinforcement significantly, which will worsen the mechanical properties of the composites [3]. With the aim of controlling the precise distribution of the super-hard B_4C particles into the soft Al matrix, the powder metallurgy (P/M) process is focused in this work. The P/M route has potential advantages in (1) easing the harmful interfacial reaction between the matrix and reinforcement; (2) improving the possibility of adding higher amounts of reinforcement; (3) controlling the microstructure of the phases. Mechanical alloying (MA) is one of the P/M processes that produce uniform dispersion of the reinforcement particles in the matrix, which help to avoid the reinforcement clustering of agglomerates on the matrix, especially when the reinforcement particles size is small. By using the high-energy ball milling technique during the mechanical alloying process, a severe plastic deformation was imparted on the powder, leading to structural refinement by shear and the fracture of the powder mixtures and the re-crystallization process. The MA process is based on repeating welding-fracturing-welding of powder mixtures in a high-energy ball mill [3].

In the present work, the powder mixtures of Al and B_4C were ball-milled at different energy levels followed by pressing, sintering, hot-extrusion, and hot-rolling to improve the mechanical and neutron absorption properties of the B_4C-Al composite. It is well known that the nuclide boron-10 (B-10) has a large thermal neutron absorption cross section above 3800 barns [11–14]. To apply the B_4C-Al composites in nuclear industry, the urgent issue is the neutron absorption ability which is closely related to the safety of nuclear plants. For the B_4C-Al composites prepared in this study, the distribution of the B_4C particle could affect the properties of the thermal neutron absorption of the composite materials, which is mainly due to the differences of B-10 density in the matrix. Neutron radiography analysis with thermal neutrons is often used as a nondestructive inspection technique to acquire the distribution of micrometer and submicrometer-sized structures in bulk samples, and it can reveal the distribution of elements such as Al, B, and C in a depth of centimeter level [16,17]. In this study, the distribution of the B_4C particle inside the Al matrix was studied using neutron radiography. It was revealed that the high-energy ball milling was crucial to the uniform distribution of the B_4C particles and the enhancement of the mechanical properties of the B_4C-Al composite plates.

2. Materials and Methods

Commercial powders of boron carbide (B_4C, ≥95.0% purity, Jingangzuan Boron Carbide company Ltd., Mudanjiang, China) and aluminum (99.5% purity, Northeast Light Alloy Company Ltd., Haerbin, China) were used in this study. The microstructural morphology of the powders was investigated using a scanning electron microscope (SEM, Camscan Apollo 300). As shown in Figure 1, the B_4C powder has a particle size of less than 10 μm with a polygonal morphology. The aluminum powder has a particle size of less than 100 μm with an ellipsoidal shape (Figure 2). From the inset picture in Figure 2, Al powders are actually made up of many particles with diameters less than 5 μm. Energy dispersive X-ray analysis (EDX) showed that there is a thin oxide layer covering the Al particle surface.

The as-received powder of 15 wt % B_4C-Al and 20 wt % B_4C-Al were ball-milled (Simoloyer-CM01, Zoz Gmbh, Wenden, Germany) for three hours with rotation speeds of 800 rpm (high-energy ball milling process) and 100 rpm (low-energy ball milling process). The stainless steel balls with diameters of 5 mm were used and the ball-to-mass ratio was 10:1. All the powders were milled under Ar atmosphere without any process control agent. The ball-milled mixtures were cold-pressed (DY-20,

KQGX Company Ltd., Tianjin, China) uniaxially in a cylindrical holder (Φ50 mm $\times$ 50 mm) with an external pressure of 25 MPa. The pressed samples with a theoretical density of 80% were heated in a vacuum furnace (VSF-335, Szvac Company Ltd., Shenyang, China) at 530 °C for three hours. The sintering procedures are illustrated in Figure 3. The sintered samples were hot extruded at 480 °C (with an extrusion rate of 9:1 and a extrusion speed of 1 cm·s^{-1}, YL32-1000, Yili Company Ltd., Hanyang, China) followed by a hot rolling (with a speed of 0.3 m·s^{-1}, LG-300, Yunnan Machine Tool Factory, Kunming, China) at 460 °C. The final products are plates with a thickness of 3 mm [18–22]. Sample plates prepared using the pure Al powder without B_4C particles were used as a reference for comparison.
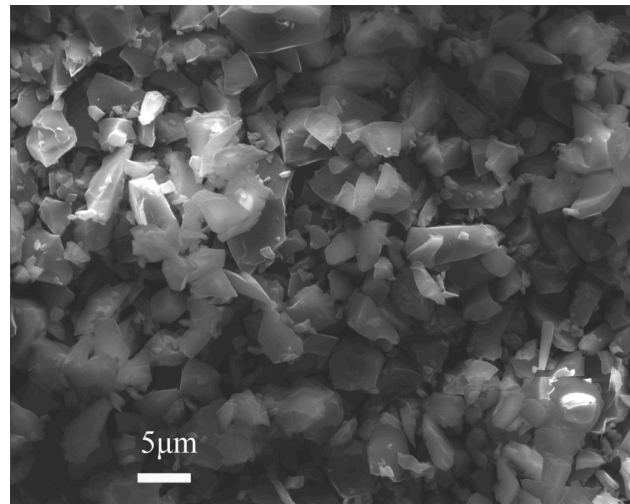

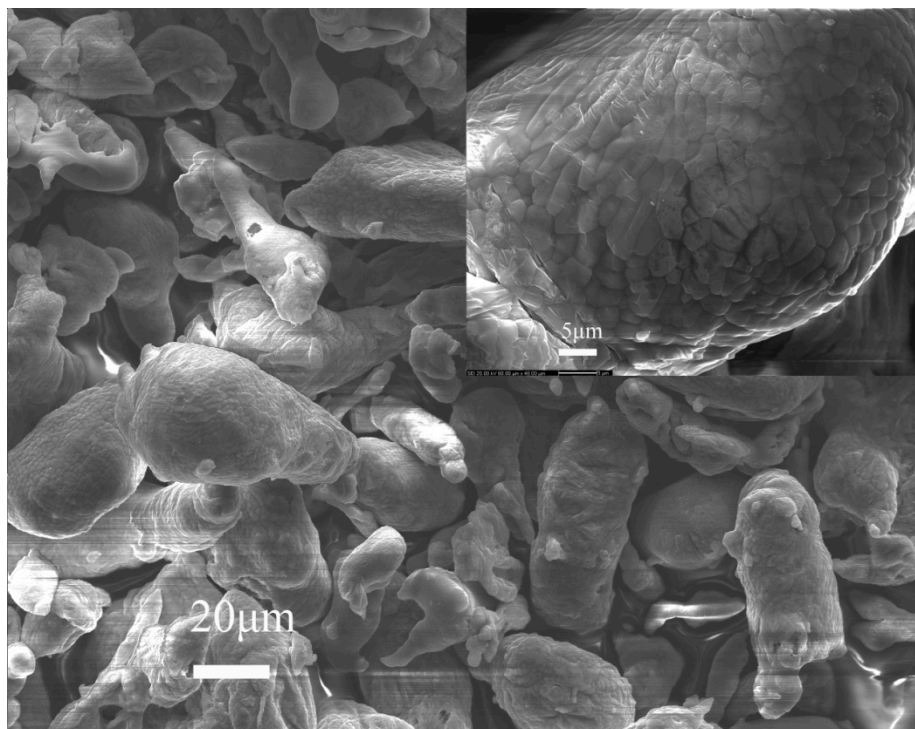**Figure 1.** Scanning electron microscope (SEM) micrograph of B_4C powders.

Figure 2. SEM micrograph of Al powders; the inset picture shows the magnified image of a single Al particle.
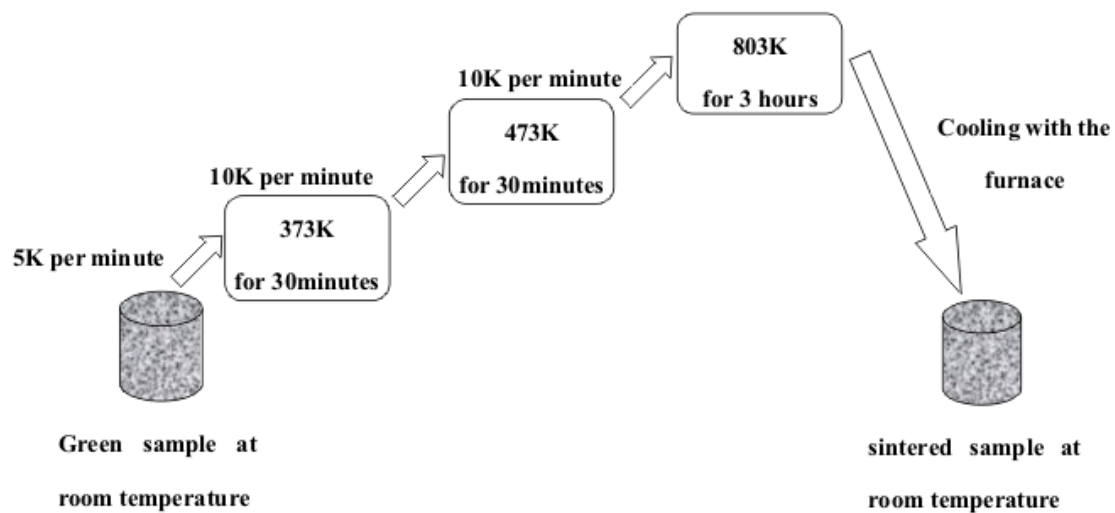
Figure 3. Sintering schedule of B_4C-Al composites.

Crystalline structures of the composites were examined by X-ray diffraction (XRD, Panalytical X'pert PRO MPD). Microstructural and fracture morphology was investigated using a scanning electron microscope (SEM, Camscan Apollo 300). Mechanical properties of the composites were studied at room temperature using a tensile test facility (MTS 810). Rectangular tensile samples were prepared according to the standard of GB/T 228-2002. The size of the tensile samples was 104 mm (L) × 22.5 mm (W) × 3 mm (T). Neutron radiography of the composites was taken along the thickness direction (normal direction, ND) in order to check the homogeneity of these composites. The neutron fluent rate was 7.8×10^7 $n \cdot cm^{-2} \cdot s^{-1}$, and the neutron energy was 0.0253 eV. The size of rectangle samples for neutron radiography was 40 mm (L) × 10 mm (W) × 3 mm (T). The center line of the all the studied samples parallels the hot-rolling direction (rolling direction, RD).

3. Results and Discussion

3.1. Microstructure Analysis

Figure 4 shows the XRD patterns of the Al powder, B_4C particulates, and as-received B_4C-Al composites prepared under different conditions. Apart from the original phases of Al and B_4C, new peaks at 41.790° and 43.079° can be assigned to those from $Al_{76.8}Fe_{24}$ [23]. Formation of the $Al_{76.8}Fe_{24}$ phases in the composites is mostly originated from (1) contamination from the steel ball; and (2) the reaction between Al powder and the Fe_2O_3 existed in the raw B_4C powders. The heating temperature of B_4C-Al composites was below the melting point of Al, hence there are no apparent ternary carbides and diborides in these composites [7,13,24].

The SEM micrographs of various B_4C-Al plates are shown in Figure 5. It is observed that the microstructure is significantly changed with the energy of ball milling. Both the 15 wt % and 20 wt % B_4C-Al composites prepared by high-energy ball milling show good bonding between the Al matrix and the B_4C particulates without apparent micro-voids at their interfaces (Figure 5c,d). However the composites prepared by low-energy ball-milling, voids and micro-voids were observed inside the matrix and at the matrix-particulate interfaces (Figure 5a,b).

Figure 6 shows the neutron radiography images of the B_4C-Al composites, in which the black areas correspond to the B_4C particles or B_4C agglomerates.
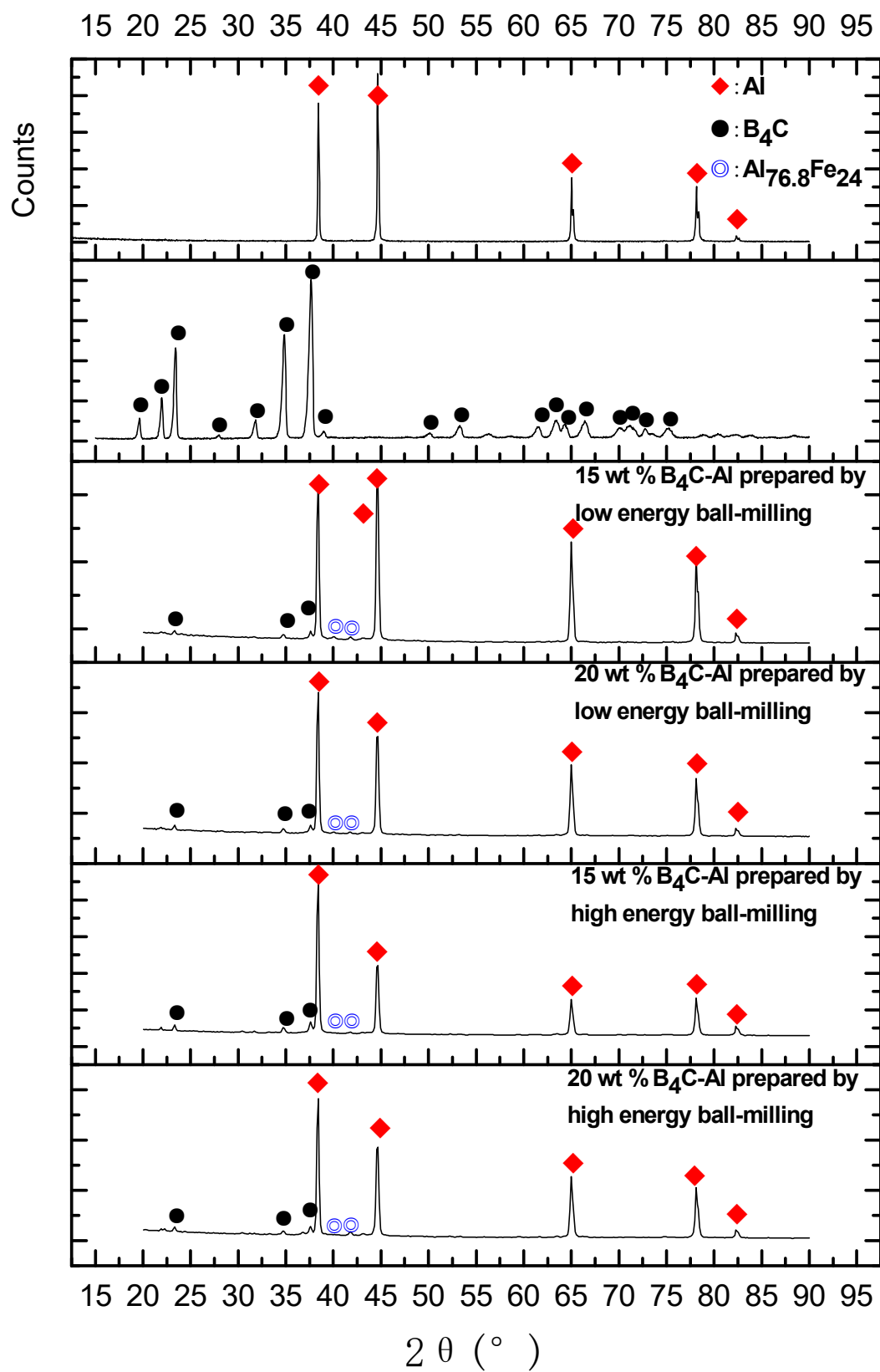
Figure 4. X-ray diffraction (XRD) patterns of the raw materials and B_4C-Al composites.
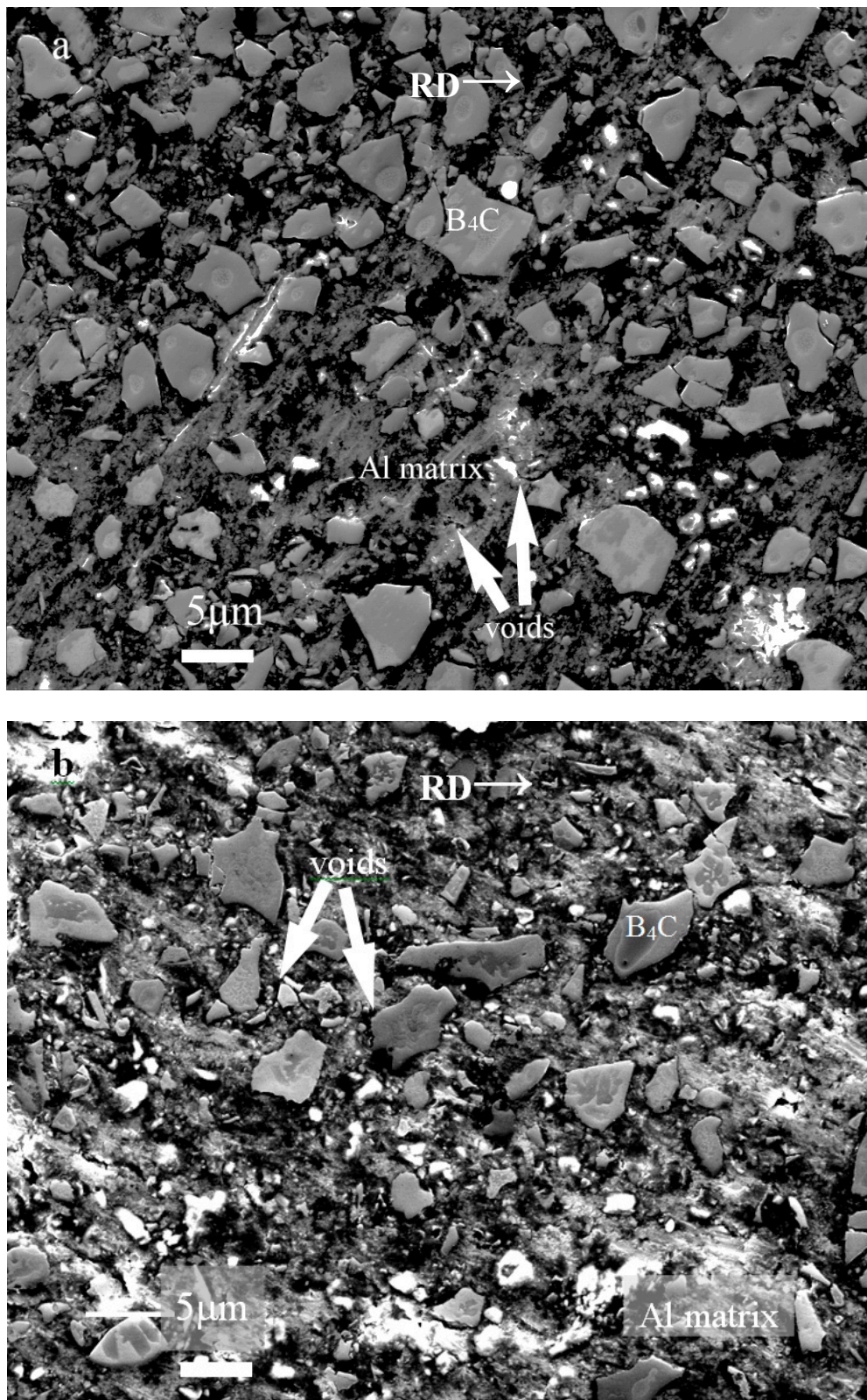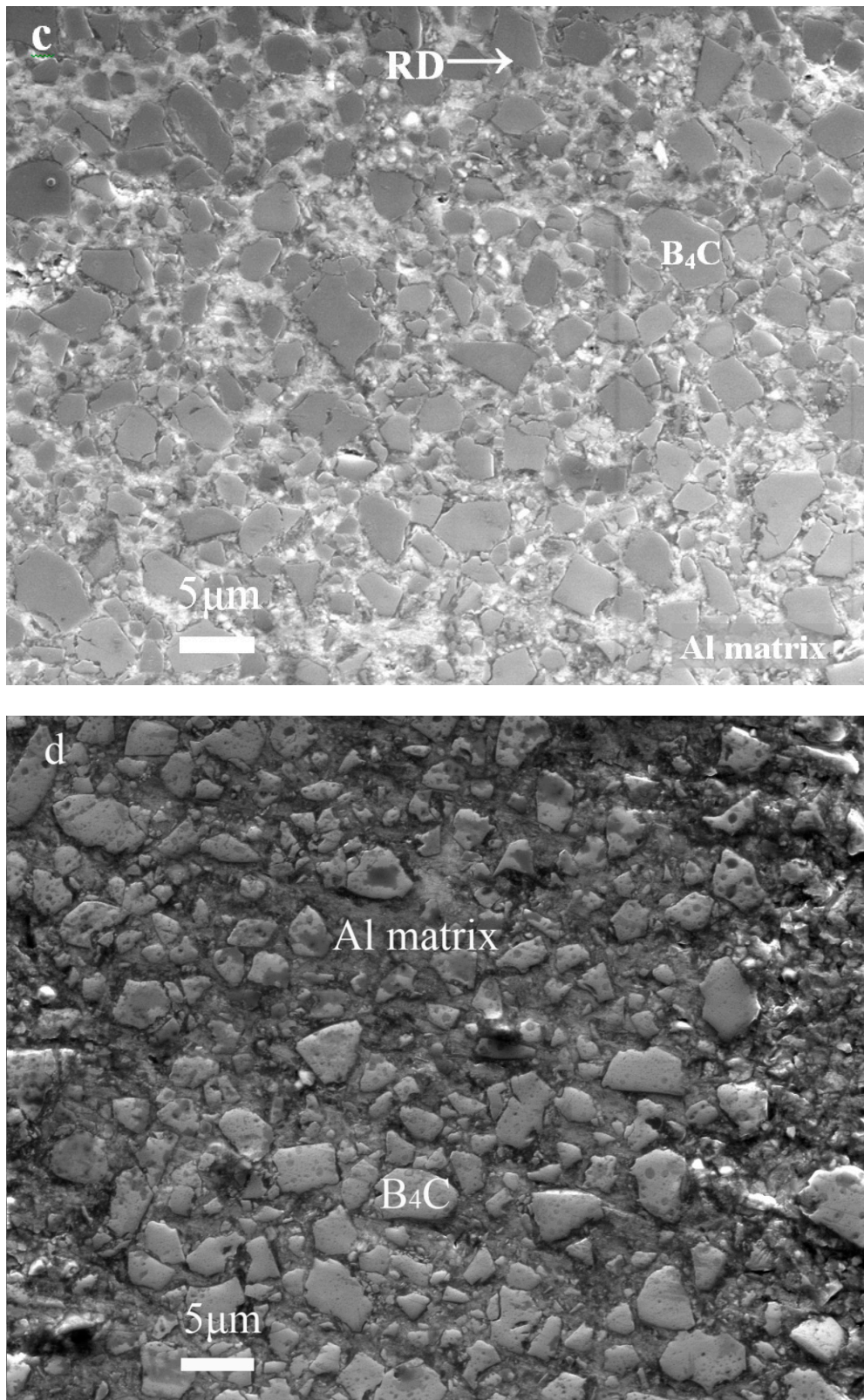
Figure 5. *Cont.*

Figure 5. SEM micrograph of polished B_4C-Al composites with various ratio of B_4C: (**a**) 15 wt % B_4C-Al prepared by low-energy ball milling; (**b**) 20 wt % B_4C-Al prepared by low-energy ball milling; (**c**) 15 wt % B_4C-Al prepared by high-energy ball milling; (**d**) 20 wt % B_4C-Al prepared by high-energy ball milling.
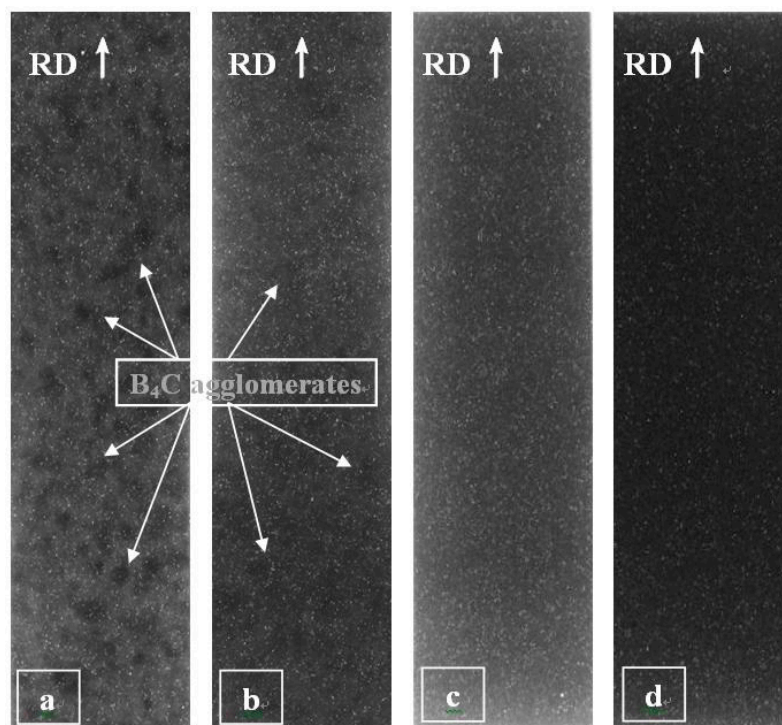
Figure 6. Neutron radiography of B_4C-Al composites: (**a**) 15 wt % B_4C-Al prepared by low-energy ball milling; (**b**) 20 wt % B_4C-Al prepared by low-energy ball milling; (**c**) 15 wt % B_4C-Al prepared by high-energy ball milling; (**d**) 20 wt % B_4C-Al prepared by high-energy ball milling.

Macroscopic B_4C agglomerates were clearly observed in the 15 wt % B_4C-Al and 20 wt % B_4C-Al composites prepared by low-energy ball milling, with estimated diameters from 0.5 mm to 1.5 mm (Figure 6a,b). As explained in the Introduction section, the microstructural non-uniformity of the B_4C particles inside the Al matrix results in the inhomogeneity distribution of B-10, thus causing the image contrast in the neutron radiography images. The images obtained from the 15 wt % B_4C-Al and 20 wt % B_4C-Al composites (shown in Figure 6c,d) prepared by high-energy ball milling reveal that the B_4C particles were dispersed uniformly inside the Al matrix, which is compared to those from the low-energy ball milling process.

3.2. Mechanical Properties

The stress-strain curves of B_4C-Al composites prepared by high-energy ball milling and low-energy ball milling processes are shown in Figure 7. Figures 8 and 9 illustrate the yield and tensile strength of the composites, respectively. The yield strength values of the 15 wt % and 20 wt % B_4C-Al composites prepared by low-energy ball milling process are 130 MPa and 141 MPa, respectively, which are ~20% and ~31% higher than those of the pure Al samples prepared at the same condition. Values of the yield strength of the 15 wt % and 20 wt % B_4C-Al composites prepared by high-energy ball milling process are 184 MPa and 213 MPa, respectively, which are ~70% and ~97% higher than those of the pure Al samples. Moreover, when increasing the ratio of the B_4C particles, the yield strength of the composite prepared by the low-energy ball milling increases slightly, whereas that of the composites prepared by high-energy ball milling increases dramatically.

As shown in Figure 9, the tensile strength of the composites prepared by the low-energy ball milling process (191 MPa and 194 MPa for 15 wt % and 20 wt % B_4C-Al composites, respectively) was almost the same as those of the pure Al samples (191 MPa) prepared using the same process. On the contrary, after high-energy ball milling, the tensile strength of 15 wt % and 20 wt % B_4C-Al composites

is significantly increased to 281 MPa and 306 MPa, which is ~47% and ~60% higher than those of the pure Al samples, respectively.
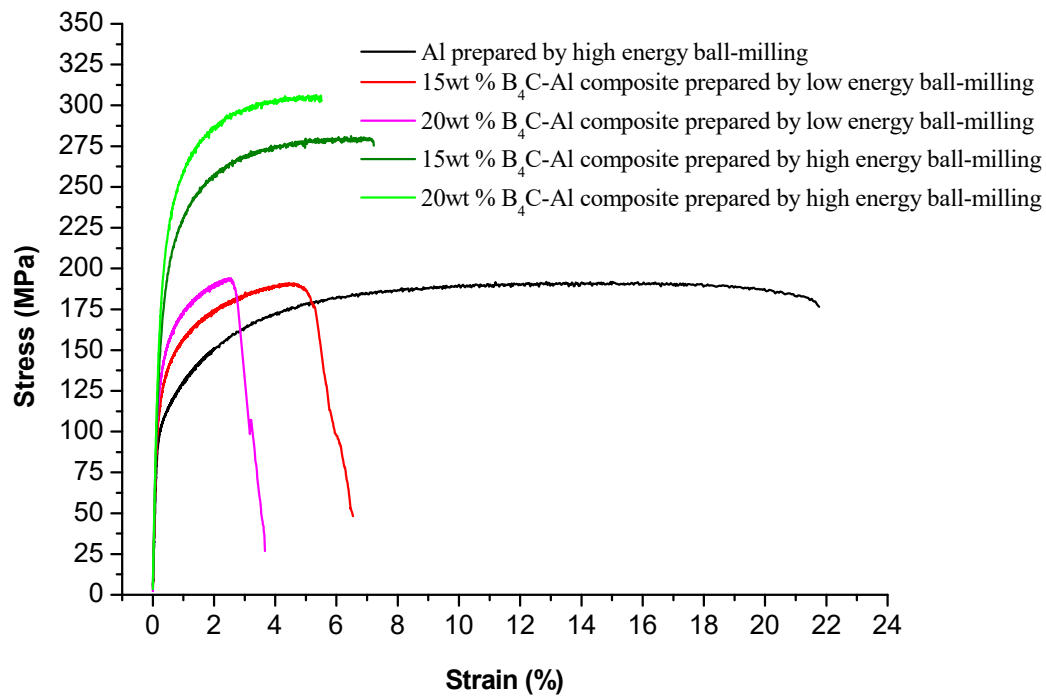

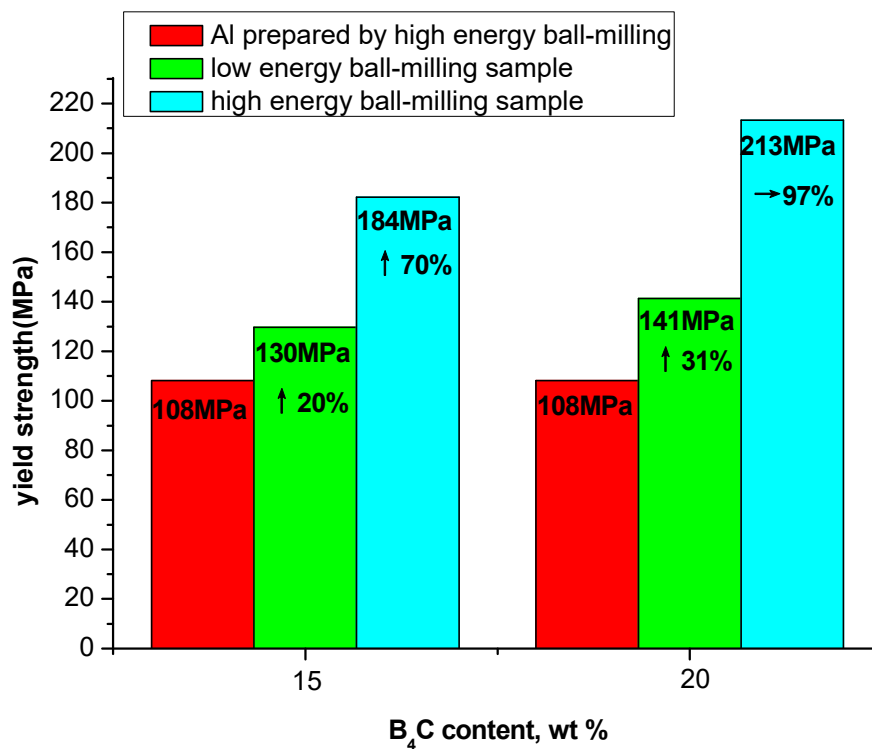**Figure 7.** The stress-strain curves of pure Al plate and B_4C-Al composites.

Figure 8. Yield strength of pure Al plate and B_4C-Al composites prepared by high-energy ball milling and low-energy ball milling.
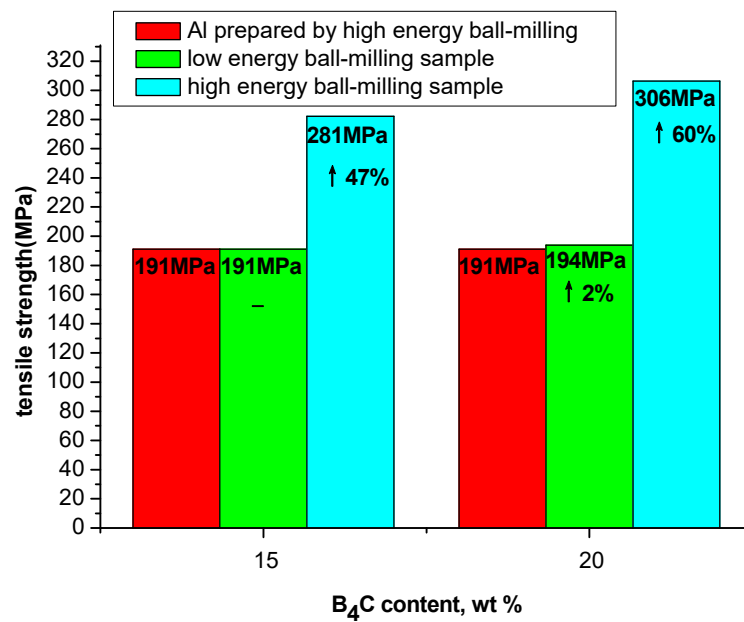
Figure 9. The tensile strength of pure Al plate and B_4C-Al composites prepared by high-energy ball milling and low-energy ball milling processes.

Figure 10 shows the SEM and the concomitant BSE images (BSTL) of the typical fracture surface of the specimens. For the sintered pure Al sample (Figure 10a), multiple shallow dimples with an average diameter of 0.8 µm are observed, which are formed by the joining of micro voids along shear slip bands. On the contrary, although the stress-strain curves of the B_4C-Al composites indicates apparent brittle fracture in a macroscopic scale without apparent necking (see Figure 7), the fracture surface morphology observed from SEM shows a ductile nature in microscopic scale with fine dimples of ~0.5 µm (Figure 10b–e). Addition of the B_4C reinforced particles reduces the macroscopic ductility, which can be verified from the formation of smaller dimples compared to those without addition of B_4C. The particle-matrix de-cohesion resulting dimples are observed, indicating that the tensile fracture of the composites is controlled by void nucleation and growth [1,25].
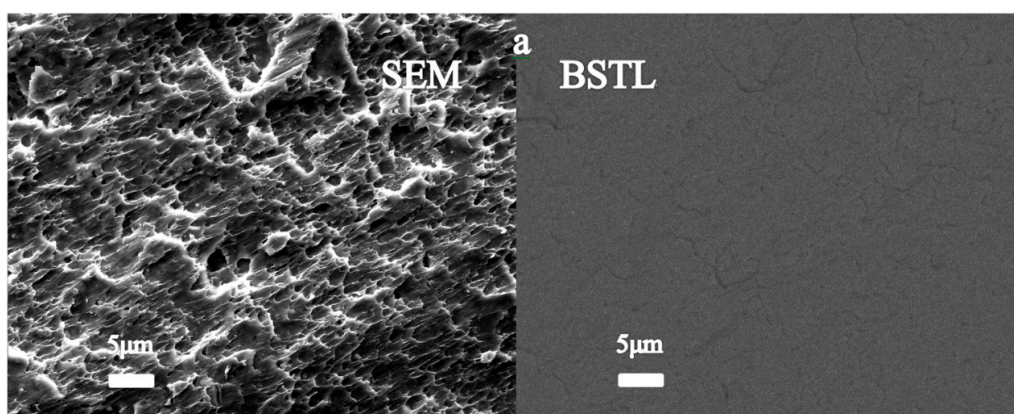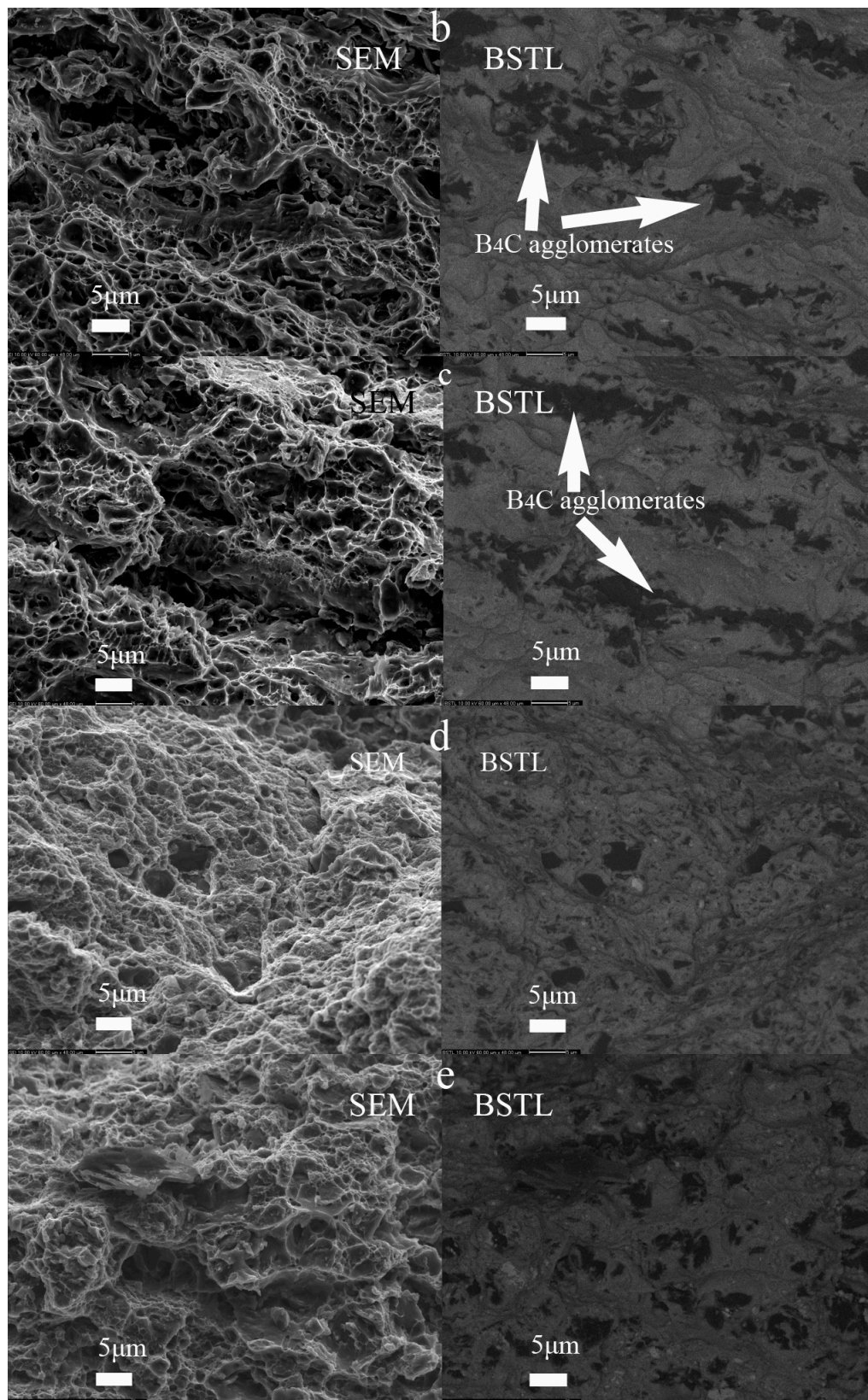

Figure 10. *Cont.*

Figure 10. Fracture surfaces of B$_4$C-Al composite: (**a**) Al without B$_4$C; (**b**) 15 wt % B$_4$C-Al prepared by low-energy ball milling; (**c**) 20 wt % B$_4$C-Al prepared by low-energy ball-milling; (**d**) 15 wt % B$_4$C-Al prepared by high-energy ball milling; (**e**) 20 wt % B$_4$C-Al prepared by high-energy ball milling.

For the composites reinforced with 15 and 20 wt % B_4C particles prepared by the low-energy ball milling process, and BSTL images reveal an inhomogeneous, stripe-like distribution of the B_4C particles (with a length of 15 μm~30 μm and a width of 4 μm~10 μm) in the Al matrix (Figure 10b,c). The agglomeration of the B_4C particles inside the Al matrix failed to transfer the shear and tensile stresses during tensile tests, blocked the movement of the slip bands, and thus lead to a de-cohesion failure of particle-matrix interfaces and fast initiation and propagation of cracks [3,25]. Consequently, the poor interfacial bonding between the Al matrix and the B_4C particles facilitates the easy crack propagation, which deteriorates the mechanical properties of the composites.

For 15 wt % and 20 wt % B_4C-Al composites prepared by the high-energy ball milling process, BSTL images reveal a homogeneous distribution of the B_4C particles (with size of ~10 μm) inside the Al matrix and a tight bonding between the B_4C particles and the Al matrix without apparent porosity (Figure 10d,e). Accordingly, the high-energy ball milling is an effective process to induce a uniform dispersion of the B_4C particles inside the Al matrix. In such cases, the load transfer from the matrix to the reinforcement is upgraded, leading to the dramatic enhancement of the yield and tensile strength of B_4C-Al composites (Figures 8 and 9). The de-cohesion of particle-matrix interfaces is facilitated and plasticity is improved (Figure 7).

Both the 15 wt % and 20 wt % B_4C-Al composites prepared by the high-energy ball milling process are stronger than those prepared by the low-energy ball milling process. XRD results show that the phases of all prepared composites are almost the same. Therefore, the differences in the mechanical properties of the composites could be attributed to the distribution of B_4C particles inside the Al matrix and the bonding between the B_4C particles and the Al matrix.

After hot extrusion and hot rolling processing, the fracture surfaces of the composites prepared by low-energy ball milling process show the apparent B_4C clusters or agglomerates inside the Al matrix, with a weak bonding between the reinforcement and the matrix (see Figures 5a,b and 10a,b). S. Sivasankaran et al. [3,26–29] reported that when the particle size of the matrix materials was considerably larger than the reinforcement particle size, the agglomeration of the reinforcement could take place, which worsened the mechanical properties of the composites and decreased the material fabricability. When the reinforcement particles were homogeneously distributed in the matrix, the P/M-processed composites showed the best characteristics, especially when the ratio of the matrix particle size to the reinforcement particle size was close to or less than unity. In this study, even though the particles size of the matrix materials is about ten times of the size of the reinforcement particle, a homogeneous distribution of B_4C particles and a good coherent bonding between the reinforcing particles and the matrix is still observed in the samples prepared by high-energy ball milling process (see Figures 5c,d and 10d,e), which contributes to the remarkable improvement of the mechanical properties of Al-B_4C composites.

These are coincident with our present tensile experiment. The deformation energy, obtained by calculating the areas below stress-strain curves, can be used to compare the tough or plastic deformation ability of the composites. As shown in Figure 7, the deformation energies of the composites prepared by high-energy ball milling process are ~1851 J·cm^{-3} and ~1524 J·cm^{-3} for 15 wt % and 20 wt % B_4C-Al composites, respectively, which are approximately an order of magnitude higher than those prepared by low-energy ball milling process (~1035 J·cm^{-3} and ~560 J·cm^{-3} for 15 wt % and 20 wt % B_4C-Al composites, respectively). It can be deduced that a homogeneous distribution of B_4C particles would increase the plastic deformation ability of B_4C-Al composites.

In brief, results indicated that the high-energy ball milling is an effective process to prevent the agglomeration of the reinforcement particles even if the matrix-to-reinforcement particle size ratio was nearly 10.

4. Conclusions

15 wt % B_4C-Al and 20 wt % B_4C-Al composites were prepared using a powder metallurgy process. Microstructure and mechanical properties of Al-B_4C composites were studied and a brief summary of the results is given below:

1. The yield strength of the 15 wt % and 20 wt % B_4C-Al composites prepared by the high-energy ball milling process is 184 MPa and 213 MPa, respectively, which are ~70% and ~97% higher than those of the pure Al samples prepared at the same condition. The tensile strength is 281 MPa and 306 MPa, respectively, which is ~47% and ~60% higher than the pure Al samples. On the contrary, the yield strength and tensile strength of the composites prepared by the low-energy ball milling process increases slightly with the B_4C particles reinforcement.
2. Microstructural, fracture surface analysis and neutron radiography indicated that composites prepared by high-energy ball milling have a homogeneous distribution of B_4C particles in the Al matrix and tight adhesions between the reinforced particles and the matrix, which give rise to better load transfer from the matrix to the reinforcement and dramatically enhance the yield and tensile strength of Al-B_4C composites.
3. High-energy ball milling is an effective process to prevent the clustering of the reinforcement particles in the matrix even if the matrix-to-reinforcement particle size ratio was nearly 10. The following pressing, sintering, hot-extrusion, and hot-rolling P/M processes are favorable to gain good adhesions between the reinforced particles and the matrix, which remarkably enhances the mechanical properties of the Al-B_4C composites.

Author Contributions: Ling Zhang designed and performed the experiment, analyzed the data, and wrote the paper; Jianmin Shi and Chunlei Shen performed the experiment together; Xiaosong Zhou contributed analysis of the data; Shuming Peng and Xinggui Long conceived the experiments.

Conflicts of Interest: The authors declare no conflict of interest.

References

1. Oñoro, J.; Salvador, M.D. High-temperature mechanical properties of aluminium alloys reinforced with boron carbide particles. *Mater. Sci. Eng. A* **2009**, *499*, 421–426. [CrossRef]
2. Toptan, F.; Kilicarslan, A. Processing and microstructural characterization of AA 1070 and AA 6063 matrix B_4C_p reinforced composites. *J. Mater. Des.* **2010**, *31*, S87–S91. [CrossRef]
3. Sivasankaran, S.; Sivaprasad, K. Synthesis, structure and sinterability of 6061 AA_{100-x}-x wt.% TiO_2 composites prepared by high-energy ball milling. *J. Alloys Compd.* **2010**, *491*, 712–721. [CrossRef]
4. Kerti, I.; Toptan, F. Microstructural variations in cast B_4C-reinforced aluminium matrix composites (AMCs). *Mater. Lett.* **2008**, *62*, 1215–1218. [CrossRef]
5. Shorowordi, K.M.; Laoui, T. Microstructure and interface characteristics of B_4C, SiC and Al_2O_3 reinforced Al matrix composites: A comparative study. *J. Mater. Process. Technol.* **2003**, *142*, 738–743. [CrossRef]
6. Yücel, O.; Tekin, A. The fabrication of boron carbide-aluminium composites by explosive consolidation. *Ceram. Int.* **1997**, *23*, 149–152. [CrossRef]
7. Mohanty, R.M.; Balasubramanian, K. Boron carbide-reinforced aluminum 1100 matrix composites: Fabrication and properties. *Mater. Sci. Eng. A* **2008**, *498*, 42–52. [CrossRef]
8. Jiang, Q.C.; Wang, H.Y. Fabrication of B_4C particulate reinforced magnesium matrix composite by powder metallurgy. *J. Alloys Compounds* **2005**, *386*, 177–181. [CrossRef]
9. Ünal, R.; Sarpün, İ.H. The mean grain size determination of boron carbide (B_4C)-aluminium(Al) and boron carbide(B_4C)-nickel(Ni) composites by ultrasonic velocity technique. *Mater. Charact.* **2006**, *56*, 214–244. [CrossRef]

10. Mashhadi, M.; Taheri-Nassaj, E. Effect of Al addition on pressureless sintering of B$_4$C. *Ceram. Int.* **2009**, *35*, 831–837. [CrossRef]

11. Viala, J.C.; Bouix, J. Chemical reactivity of aluminimu with boron carbide. *J. Mater. Sci.* **1997**, *32*, 4559–4573. [CrossRef]

12. Arslan, G.; Kara, F. Quantitative X-ray diffraction analysis of reactive infiltrated boron carbide-aluminium composites. *J. Eur. Ceram. Soc.* **2003**, *23*, 1243–1255. [CrossRef]

13. Ma, Q.-C.; Zhang, G.-J. Effect of additives introduced by ball milling on sintering behavior and mechanical properties of hot-pressed B$_4$C ceramics. *Ceram. Int.* **2010**, *36*, 167–171. [CrossRef]

14. Abenojar, J.; Velasco, F. Optimization of processing parameters for the Al + 10% B$_4$C system obtained by mechanical alloying. *J. Mater. Process. Technol.* **2007**, *184*, 441–446. [CrossRef]

15. Shi, J.M.; Shen, C.-L. Corrosion Mechanism of Al-B$_4$C Composite Materials in Boric Acid. *Atomic Energy Sci. Technol.* **2012**, *46*, 972–977.

16. Hilger, A.; Kardjilov, N. Revealing microstructural inhomogeneities with dark-field neutron imaging. *J. Appl. Phys.* **2010**, *107*, 036101. [CrossRef]

17. Scott, P.B.; Johnson, S.E. Neutron radiographs using the ionographic process. *J. Appl. Phys.* **1978**, *49*, 5078–5080. [CrossRef]

18. Zhang, L.; Shen, C.L. The Preparation of B$_4$C-Al Composites. China Patent ZL201010607497.5, 11 July 2012.

19. Shi, J.M.; Lei, J.R. Corrosion Behaviors of Al-B$_4$C Composite Materials. *Atomic Energy Sci. Technol.* **2010**, *44*, 159–165.

20. Shen, C.L.; Shi, J.M. Effect of ball milling technics on B$_4$C-Al composite performance. *Funct. Mater.* **2011**, *42*, 365–369.

21. Shi, J.M.; Zhang, L. Corrosion behavior of Al-B$_4$C composite in spent nuclear fuel storage environment. *J. Chin. Soc. Corros. Prot.* **2013**, *33*, 419–424.

22. Zhang, L.; Shi, J.M. Neutron absorption properties of Al-B$_4$C composites materials. *Mater. Rev.* **2016**, *30*, 21–25.

23. Griger, A.; Stefaniay, V. Crystallographic data and chemical compositions of aluminium-rich aluminum-iron intermetallic phases. *Z. Metallkd.* **1986**, *77*, 30.

24. Kouzeli, M.; Marchi, C.S. Effect of reaction on the tensile behavior of infiltrated boron carbide-aluminum composites. *Mater. Sci. Eng. A* **2002**, *337*, 264–273. [CrossRef]

25. Dutt, B.S.; Babu, M.N. Influence of microstructural inhomogeneities onf the fracture toughness of modified 9Cr-1Mo steel ant 298–823K. *J. Nucl. Mater.* **2012**, *421*, 15–21. [CrossRef]

26. Torralba, J.M.; da Costa, C.E. P/M aluminum matrix composites: An overview. *J. Mater. Process. Technol.* **2003**, *133*, 203–206. [CrossRef]

27. Slipenyuk, A.; Kuprin, V. The effect of matrix to reinforcement particle size ratio (PSR) on the microstructure and mechanical properties of a P/M processed AlCuMn/SiC$_p$ MMC. *Mater. Sci. Eng. A* **2004**, *381*, 165–170. [CrossRef]

28. Slipenyuk, A.; Kuprin, V. Properties of P/M processed particle reinforced metal matrix composites specified by reinforcement concentration and matrix-to-reinforcement particle size ratio. *Acta Mater.* **2006**, *54*, 157–166. [CrossRef]

29. Bhanu Prasad, V.V.; Bhat, B.V.R. Structure-property correlation in discontinuously reinforced aluminium matrix composites as a function of relative particle size ratio. *Mater. Sci. Eng. A* **2002**, *337*, 179–186. [CrossRef]